CONF-961009--6

THERMAL SPRAY DEPOSITION AND EVALUATION OF LOW-Z COATINGS*

Roland D. Seals, Catherine J. Swindeman, Rickey L. White
Oak Ridge Centers for Manufacturing Technology
Thermal Spray Technology Laboratory
Oak Ridge, TN 37831

Abstract

Thermally-sprayed low-Z coatings of boron carbide (B_4C) on aluminum substrates were investigated as candidate materials for first-wall reactor protective surfaces. Comparisons were made to thermally-sprayed coatings of boron, $MgAl_2O_4$, Al_2O_3, and composites. Graded bond layers were applied to mitigate coefficient of thermal expansion mismatch. Microstructures, thermal diffusivity before and after thermal shock loading, steel ball impact resistance, CO_2 pellet cleaning and erosion tolerance, phase content, stoichiometry by Rutherford backscattering spectroscopy (RBS), and relative tensile strengths were measured.

THERMALLY-SPRAYED BORON CARBIDE, $B_{12}C_3$ (or for simplicity, B_4C), coated aluminum panels are desirable candidate front-wall surfaces for experimental facilities used to demonstrate ignition in inertial confinement fusion (ICF) (1,2). B_4C is a low atomic number, low-density material with a high melting temperature, good thermal conductivity, and high specific heat resulting in excellent survivability against directed energy threats and cold X-rays. Enhancing the survivability characteristics of B_4C surfaces in specialized environments, such as fusion reactor target chambers, are low thermal expansion and good mechanical properties including high hardness, strength, and modulus. Front-wall target chamber surfaces must withstand exposures to high fluences of X-rays, scattered laser light, and debris. The front-wall components must also be producible and cost-effective, have low erosion from CO_2 cleaning, have low vacuum outgassing, and have high thermal shock resistance.

However, the high melting point, high specific heat, and high melting enthalpy of B_4C make it very difficult to melt by means of thermal spraying. Boron carbide does not melt congruently (3,4); that is, molten material in contact with solid becomes increasingly richer in carbon as melting progresses. Fortunately, extremely rapid solidification in the thermal spray process can reduce this effect. Another problem is the variation in cooling rate associated with particle size variation which leads to residual stress differences from splat to splat unless means are taken to prevent this occurrence.

The structure of the range of boron carbide compositions is rhombohedral (5). Compound compositions can range from B_4C at 78.25 wt% boron to at least $B_{6.5}C$ at 85.4 wt% boron. Boron carbide products, containing more carbon than the pure B_4C phase (about 21.6 wt%), exist as mixtures of boron carbide and graphitic carbon. Most boron carbide powder has at least 2.25% carbon beyond the stoichiometric limit for B_4C.

The present work addresses the development of a thermal spray process to deposit B_4C using atmospheric plasma spray (APS) without cryogenic cooling of the substrate. The objective is to develop a cost-effective thermal spray deposition process to deposit B_4C onto aluminum panels for evaluation and effects testing relative to ICF requirements. In previous work, B_4C coatings were produced by plasma spraying in inert gas at atmospheric pressure with liquid argon cooling (2) and in an inert gas atmosphere up to 2 bar (6,7).

Experimental Procedure

The low-Z coatings were deposited by APS using a Miller-Thermal 4500 System with a SG100 gun. The coating materials were plasma-sprayed B_4C, boron, $MgAl_2O_4$, Al_2O_3 and composites, and high-velocity oxy-fuel (HVOF) deposited Al_2O_3. The coatings were deposited on 5083 aluminum coupons coated with graded bond coats to mitigate thermal expansion differences. The list of materials is given in Table I. After the coating deposition parameters were determined for each material, 24 coupons [12.7-mm (0.5-in.) diam.]

*Research sponsored by the U.S. Department of Energy, under contract DE-AC05-84OR21400 with Lockheed Martin Energy Systems, Inc.

Table I. Thermal spray coatings on 5083 aluminum substrates

Top coat[1,2]	Graded bond coat[1]
Al_2O_3	75 Al_2O_3–25 Al/100 Al
B_4C	75 Al_2O_3–25 Al/100 Al
90 B_4C–10 Al_2O_3	75 Al_2O_3–25 Al/100 Al
50 B_4C–50 C	75 Al_2O_3–25 Al/100 Al
90 C–10 Al	75 C–25 Al/100 Al
90 C–10 Al_2O_3	75 C–25 Al/100 Al
$MgAl_2O_4$	75 $MgAl_2O_4$–25 Al/100 Al
HVOF Al_2O_3	-------No bond coat----------

[1]Feed rate composition by weight percent.

[2]Feed rate composition by weight percent for sprayed powder; for coating composition see text.

were simultaneously coated for X-ray testing and microstructural, relative tensile strength, phase content, Rutherford backscattering spectroscopy (RBS), and thermal shock evaluations. Additionally, 14 coupons 10.2 cm^2 (4 $in.^2$) were simultaneously coated with each material for testing of impact resistance, CO_2 cleaning erosion tolerance, and vacuum outgassing.

Tensile strength testing was completed following American Society for Testing and Materials (ASTM) 633C procedures with the exception that 12.7-mm-diam. (0.5-in.) samples were used. Tensile strength of thermally-sprayed aluminum butt tensile specimens was evaluated using an Instron machine. The specimens had been grit blasted with aluminum oxide followed by cleaning in 5% Brulin 815GD at 55°C in a 20-kHz ultrasonic cleaner, rinsing in flowing demineralized water, and air drying. The samples were bonded using 2.08 g of Armstrong A-12 part A epoxy resin with 2.13 g Armstrong A-12 part B epoxy curing agent. After hand mixing the epoxy for ~1 min and vacuum degassing, 0.02 mL of the epoxy was applied with a microsyringe to the coated butt tensile specimen. A second butt tensile specimen was force applied until the epoxy was seen at the edges. The samples were then wrapped in mylar to ensure alignment, and weights were placed on top of the specimens to ensure uniform bonding. After curing for sufficient time at room temperature, the samples were tested using an Instron machine.

The RBS data were supplied by M. Tobin of Lawrence Livermore National Laboratory (LLNL). RBS spectra were acquired using a He^{++} ion beam energy of 2.275 MeV at a backscattering angle of 160° with the sample perpendicular to the incident ion beam.

Thermal shock resistance was evaluated by measuring thermal diffusivity before and after thermal loading. To thermal load the coatings, the samples were preheated to 150°C for a minimum of 20 min and then submerged in water at 0°C for a minimum of 3 min. The samples were removed from the water, placed on clean dry towels, air dried, and finally vacuum outgassed for 12 h. The differences between the prethermal and postthermal diffusivity were noted. Thermal diffusivity values were measured by using a xenon flash lamp to heat the front side of the coatings and an infrared (IR) detector to detect the substrate backface temperature response.

Steel spheres of different mass were dropped on the 10.2-cm^2 (4-$in.^2$) plasma-spray-coated aluminum plates supported on two opposing edges to assess low-velocity impact tolerance. The plates were impacted with successively larger mass spheres.

The X-ray testing was coordinated by M. Tobin of LLNL and performed using the French Phebus facility at CEA/DAM Centre D'Etudes De Limeil-Valenton.

Results and Discussion

The plasma spraying parameters used for B_4C and Al_2O_3 are outlined in Table II. Plasma spraying of B_4C coatings required argon jet shrouds and a standoff distance of 50.8 mm (2.0 in.). The argon jets [3.18-mm (0.125-in.) copper tubing] were directed toward the molten drops just before impact. The intent of this approach was to attain a more uniform cooling rate for the molten particles, thus reducing the carbon concentration redistribution and residual stresses within the solidified splats.

Table II. Plasma spray parameters using a SG100 gun

Parameter	Al_2O_3	B_4C
Arc gas	Ar/He	Ar/He
Gas flow rate (scfh)	82/40	70/40
Arc current (A)	900	1100
Arc voltage (V)	47.2	46.9
Carrier gas	Ar	Ar
Gas flow rate (scfh)	15	15
Powder feed rate (g/min)	10	12
Argon jet shroud	No	Yes
Standoff (in.)	3	2
Substrate cooling	Yes	No

Graded bond coats were used to mitigate significant differences in the coefficients of thermal expansion between the aluminum substrates and the ceramic coatings. Thermal expansion coefficients are 24 to 27 $\times 10^{-6}$/°C for aluminum and $<8 \times 10^{-6}$/°C for the ceramics. The bond coat was graded (see Table I) from 100% aluminum to 75% ceramic–25% aluminum for plasma-sprayed B_4C, B_4C composites, boron, and Al_2O_3 coatings; 100% aluminum to 75% $MgAl_2O_4$–25% aluminum for plasma-sprayed $MgAl_2O_4$ coatings; and 100% aluminum to 75% carbon–25% aluminum for the 90% carbon–10% aluminum composite coating. A bond coat was not used for the HVOF-deposited Al_2O_3. The graded bond coat interface for a B_4C coating is shown in the scanning electron microscopy (SEM) photomicrographs of a polished cross-section in Fig. 1. The boron and aluminum X-ray elemental

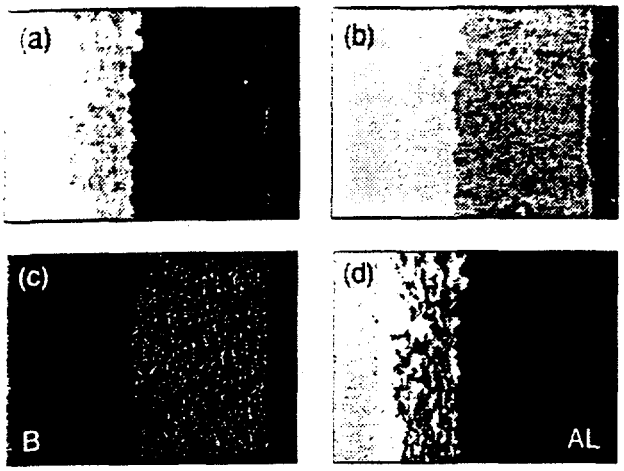

Fig. 1. Plasma-spray-deposited B_4C/graded bond coat/aluminum substrate: (a) SEM backscattered electron image; and (b) secondary electron image; and the corresponding elemental mapping for (c) boron and (d) aluminum.

maps are also shown. Typical thicknesses of the coatings are given in Table III.

X-ray diffraction (XRD) analysis of the plasma-sprayed ceramic coatings indicated that the grains were randomly oriented, as evidenced by the excellent match between the experimental diffraction intensities and those from the powder diffraction file (PDF). The XRD pattern for B_4C as shown in Fig. 2 indicated minor phases of boric acid [$B(OH)_3$] and boric oxide (B_2O_3). When attempts were made to plasma-spray a 50:50 wt% mixture of B_4C and carbon, the results from XRD and RBS analyses were identical to that for plasma-sprayed B_4C samples, indicating that the carbon did not alter the boron carbide phase equilibrium. However, there was no evidence of excess carbon in the coating. The XRD analysis of the plasma-sprayed Al_2O_3 indicated equal amounts of alpha-Al_2O_3 and gamma-Al_2O_3 phases. The broad XRD lines for the gamma phase indicate poor crystallinity. The XRD pattern for plasma-sprayed $MgAl_2O_4$ revealed the major phase as spinel with a trace of aluminum. The spinel lines were broad, possibly indicating strain or compositional variation. Comparison with the standard PDF showed a decrease in the lattice parameter, possibly indicating a slight compositional change. The XRD results for plasma-sprayed boron coatings indicated beta-rhombohedral boron (not the room temperature stable alpha phase) and a minor amorphous component.

Table III. Typical layer thicknesses of the thermal sprayed coatings from optical microscopy measurements

Top coat	Top coat [μm (in.)]	Bond coat [μm (in.)]	Total [μm (in.)]
Al_2O_3	381 (15.0)	274 (10.8)	655 (25.8)
B_4C	403 (15.9)	269 (10.6)	672 (26.5)
90 B_4C–10 Al_2O_3	397 (15.7)	273 (10.7)	670 (26.4)
50 B_4C–50 C	583 (23.0)	215 (8.4)	798 (31.4)
90 C–10 Al	–	–	700 (27.6)
90 C–10 Al_2O_3	427 (16.8)	241 (9.5)	668 (26.3)
$MgAl_2O_4$	447 (17.6)	217 (8.5)	664 (26.1)

RBS results for plasma spray coatings of B_4C and 50:50 weight ratio B_4C–C were 79.1 at% boron, 19.5 at% carbon, and 1.0 at% oxygen compared to stoichiometric amounts of 80% boron–20% carbon and 66.7 at% boron–33.3 at% carbon.

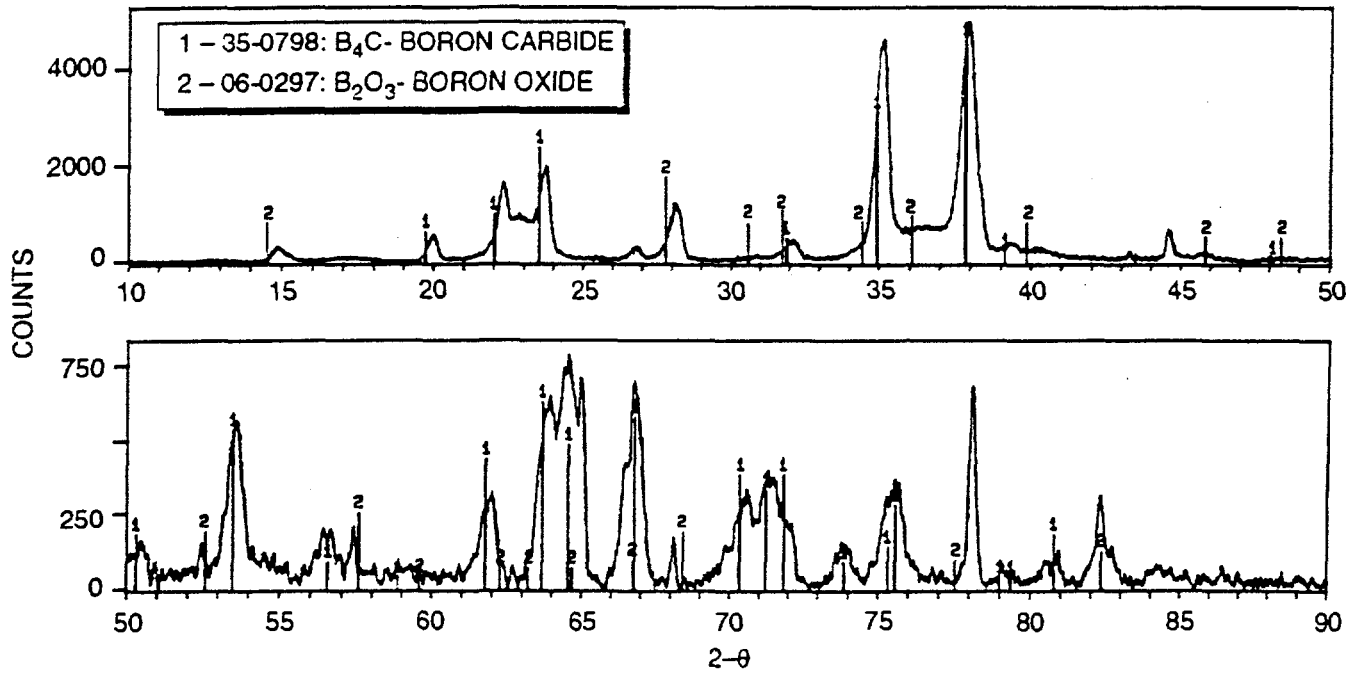

Fig. 2. XRD pattern for plasma-spray-deposited B_4C.

respectively. The results indicated that carbon did not build up in the matrix and that the B_4C–C composite coating did not result with this approach. The carbon used in the experiments was spherical glassy carbon powder. However, when a 10:90 weight ratio mixture of Al_2O_3–C was plasma sprayed, the coating contained 6.2 wt% of carbon. The resulting composition according to RBS analysis was 35.9 at% aluminum (14.3), 53.8 at% oxygen (21.4), and 10.0 at% carbon (64.3) compared to the stoichiometric amounts shown parenthetically for the 10:90 wt% mixture. Similar results were obtained when a 10:90 weight ratio of aluminum–carbon was plasma sprayed. The RBS results for a plasma-sprayed 90:10 weight ratio of B_4C–Al_2O_3 were 73.0 at% boron (72.0), 18.0 at% carbon (18.0), 3.6 at% aluminum (4.0), and 5.4 at% oxygen (6.0) compared to the stoichiometric amounts shown in parentheses.

Erosion tolerance evaluations were conducted using a CO_2 centrifuge pellet accelerator mounted on a Fanuc S-420F robot. The centrifuge pellet accelerator allowed excellent control of the pellet energy and mass impacting the coating surfaces per unit area. The 10.2-cm^2 (4-$in.^2$) samples were impacted with measured amounts of pellets at specific rotor speeds along stationary lines 16 mm apart. The test pattern used for each sample is shown in Fig. 3, and the test parameters, for example, pellet speeds, amounts, and energies, are given in Table IV. Surface cleaning of the weakly bound particles occurred for CO_2 pellet erosion of B_4C and Al_2O_3 coatings at a rotor speed of 6,000 rpm, which corresponds to a pellet speed of 175 m/s and energy of 7 kJ. Slight removal of surface coating material occurred for rotor speeds of 8,000 and 10,000 rpm. Complete removal of the surface coating material leaving only the graded bond coat resulted at 12,000 rpm (CO_2 pellet speed of 351 m/s and energy of 28 kJ) for CO_2 pellet erosion of the Al_2O_3 coating shown in Fig. 4. Under the same conditions, the B_4C surface coating was partially removed as shown in Fig. 4. Complete removal of the $MgAl_2O_4$ surface coating leaving the graded bond coat occurred at rotor speeds

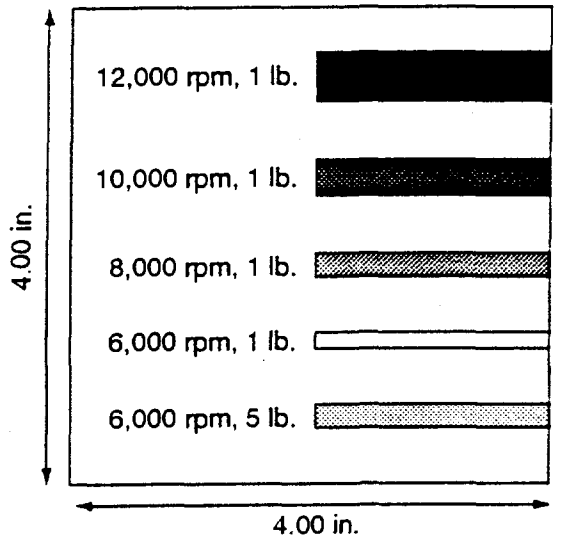

Fig. 3. CO_2 pellet accelerator test pattern.

Table IV. CO_2 centrifuge pellet accelerator test levels

Rotor speed (rpm)	Pellet speed [m/s (ft/s)]	Amount (kg)	Total energy (kJ)
12,000	351 (1,150)	0.91	56
12,000	351 (1,150)	0.45	28
10,000	292 (958)	0.45	19
8,000	234 (767)	0.45	12
6,000	175 (575)	2.27	35
6,000	175 (575)	0.45	7

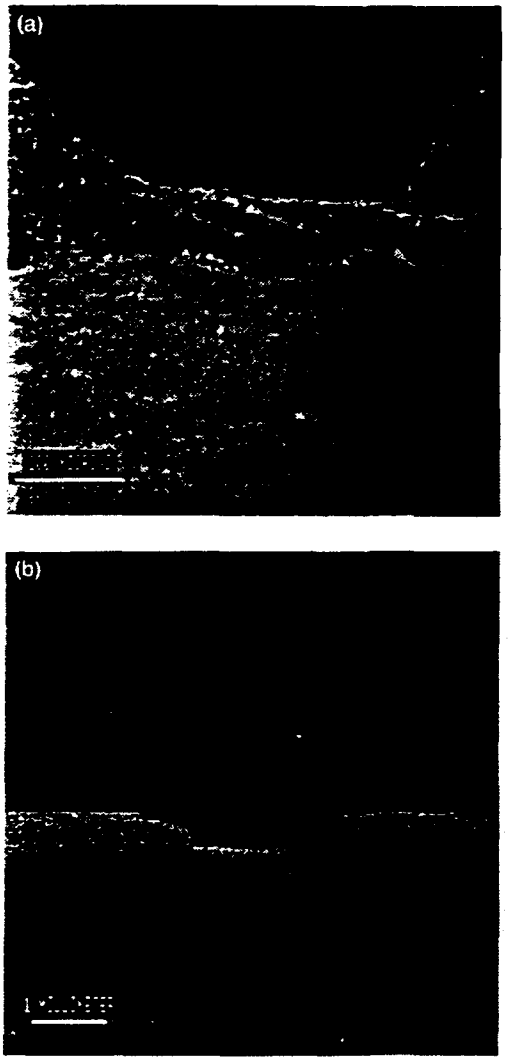

Fig. 4. SEM secondary electron image of CO_2 pellet erosion at a pellet speed of 351 m/s and energy of 28 kJ; (a) B_4C and (b) Al_2O_3.

of 10,000 rpm and 12,000 rpm with the width of the damaged area at 12,000 rpm matching the width of the impacted pellet stream. For composite coatings using starting powders of 75carbon–25Al_2O_3, 50carbon–50B_4C, and 90B_4C–10Al_2O_3 (wt %), surface cleaning occurred at rotor speeds of 6,000 and

5,000 rpm, some surface coating removal occurred at 10,000 rpm, and complete removal of the surface coating down to the bond coating occurred at 12,000 rpm.

Relative tensile strength values of the 12.7-mm (0.5-in.) coated samples are shown in Fig. 5. Five samples were measured for each coating. The values were ranked relative to butt tensile specimens plasma-sprayed with Al_2O_3. Tensile strengths for specimens sprayed with graded bond coats are also shown in Fig. 5. Failure occurred in the coating or at the interface between the coating and the substrate for each specimen. The relative ranking of the tensile strengths of the coatings are Al_2O_3 > 90%carbon–10%Al_2O_3 > 90%B_4C–10%Al_2O_3 > 90%carbon–10%aluminum > 50%B_4C–50%carbon > B_4C > $MgAl_2O_4$ > HVOF Al_2O_3. Tensile strength values of the composite coatings of plasma-sprayed 90%carbon–10%Al_2O_3, 90%B_4C–10%Al_2O_3, and 90%carbon–10%aluminum were proportional to the resultant coating composition. The HVOF Al_2O_3 coating did not have a graded bond coating, which is evident in the results.

The thermal shock resistance of the coatings was evaluated by measuring thermal diffusivity before and after thermal shock loading with a 150°C to 0°C temperature drop. Thermal diffusivity is the speed at which heat flows from a region of higher temperature to the surrounding material. Thermal diffusivity values were measured by using a xenon flash lamp to heat the front side of the coatings and an IR detector to detect the substrate backface temperature response.

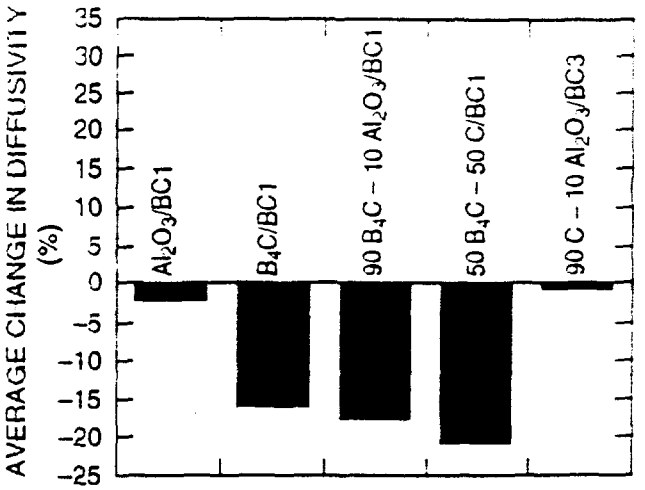

Fig. 6. Thermal shock resistance.

The thermal diffusivity was calculated from the equation:

$$\alpha = (0.1388\ d^2)/(t_{1/2}) \qquad (1)$$

where α is the thermal diffusivity, d is the sample thickness, and $t_{1/2}$ is the rise time at the half peak value of the IR detector output. The difference between the prethermal and post-thermal diffusivity was noted for five different samples of each coating material.. The change in thermal diffusivity noted for B_4C and B_4C composite coatings suggests that either a small amount of delamination or microcracking within the

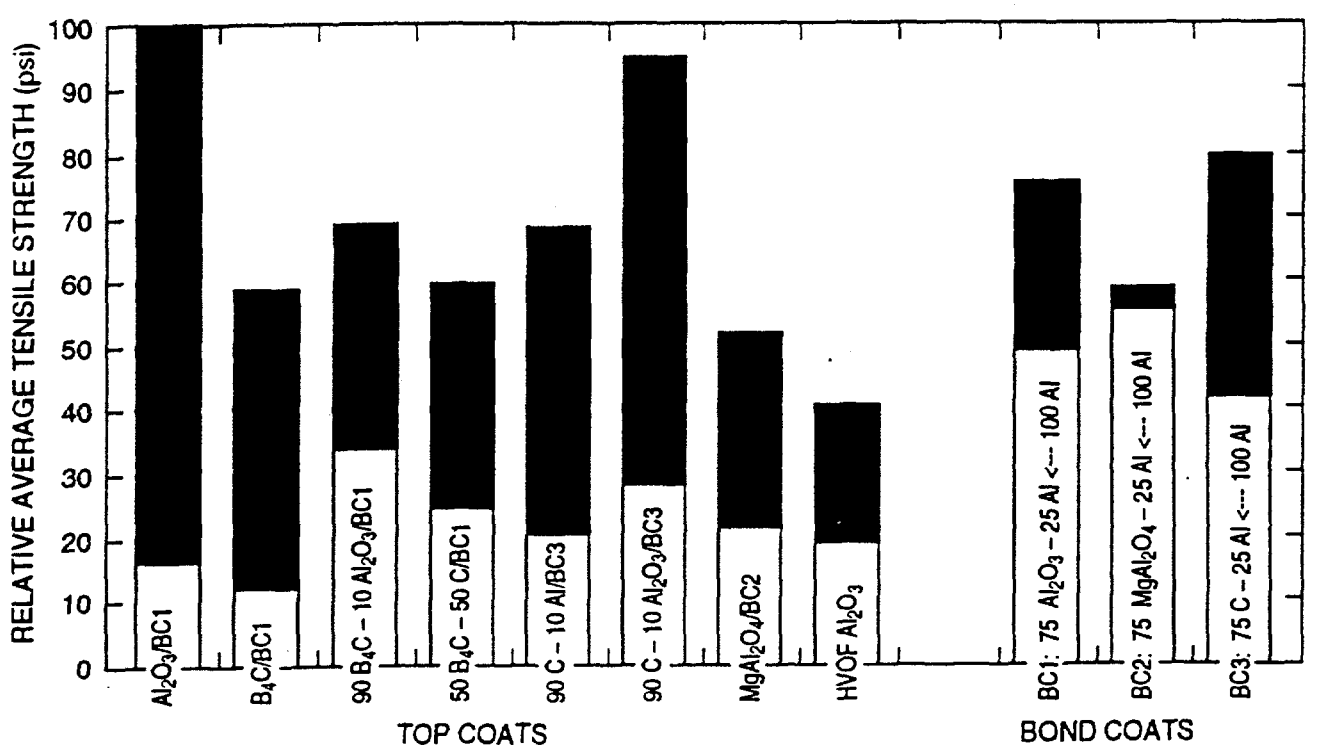

Fig. 5. Relative tensile strengths.

coating occurred due to thermal loading. Mechanical strengths, erosion resistance, and X-ray tolerance of the B_4C coatings should also be evaluated after thermal shock treatments, but were not in this study.

Low-velocity impact tests were performed by dropping various steel spheres of different mass from 3 m onto 10.2-cm^2 (4-in.^{2}) plasma-spray-coated aluminum plates (five samples each). The plates were supported on two opposing edges and were impacted with spheres of successively larger mass. The mass of the steel impactors ranged from 1 g to 1 kg with a velocity of 6.25 m/s. This translated to a momentum of 6.25 kg•m/s and a kinetic energy of 0.02 to 20 Nm. The momentum of incipient spallation for each coating is shown in Fig. 7. All of the coatings exhibited incipient spallation at ~2.8 kg•m/s with the exception of the C–Al composite (no spallation) and $MgAl_2O_4$ coating (much lower). The cumulative inelastic deflection vs the momentum is given in Fig. 8. The momentum was greater than 4 kg•m/s before the cumulative inelastic deflection exceeded 1.0 mm for B_4C and B_4C composite coatings. The coatings exhibited comparable impact performance with the exception of the C–Al composite coating, which performed at the greatest impact tolerance. The $MgAl_2O_4$ showed the least impact tolerance. Impact damage ranged from slight surface compression to significant spallation. For example, at a drop of 3 m, steel sphere mass of 1.044 kg, velocity of 7.66 m/s, and momentum of 8.00 kg•m/s, the plasma-sprayed coating of the C–Al composite material showed only slight surface compression and no spallation; the coatings of plasma-sprayed Al_2O_3 and HVOF Al_2O_3 materials showed slight surface compression and little spallation; and the B_4C, Al_2O_3–B_4C composite, Al_2O_3–C composite, and

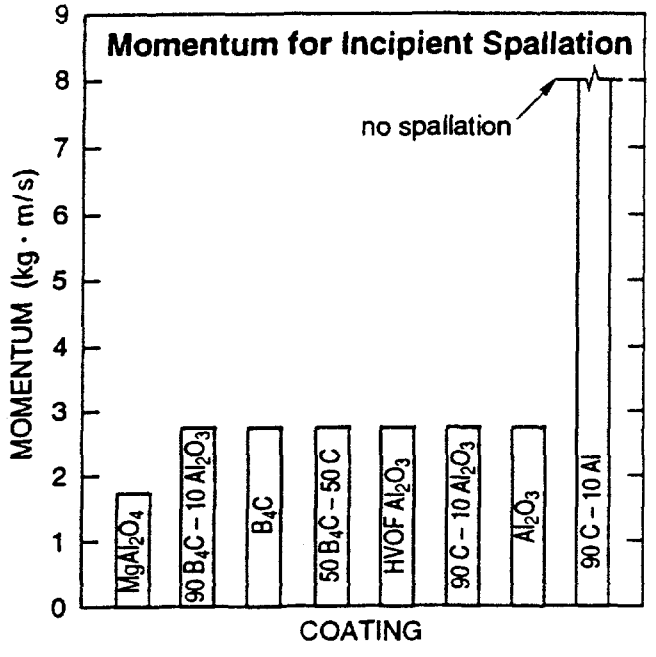

Fig. 7. Momentum of incipient spallation from low-velocity impact of steel spheres.

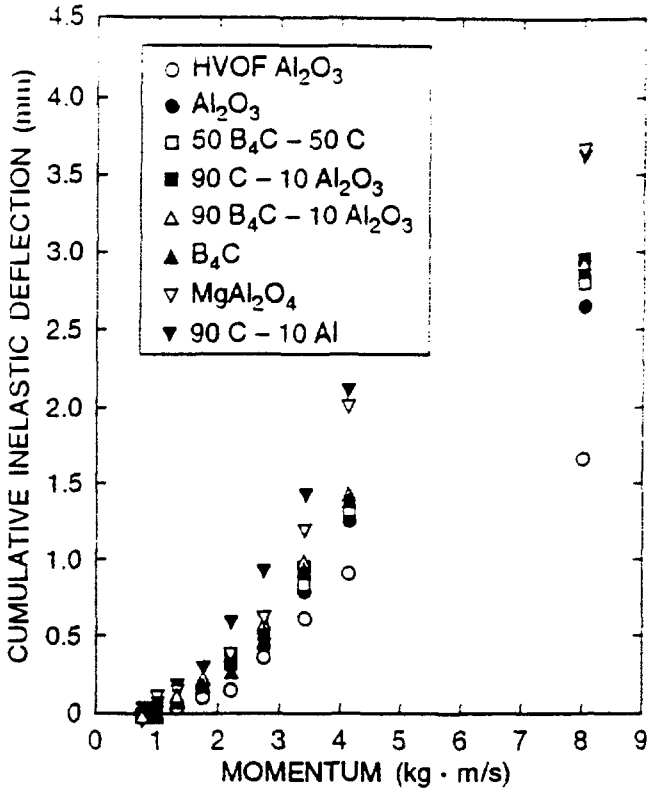

Fig. 8. Cumulative inelastic deflection vs momentum for low-velocity impact of steel spheres.

B_4C–C composite materials showed some spallation and coating cracking parallel to the edge supports. The $MgAl_2O_4$ coating showed extensive spallation. Performance of the coatings to cumulative inelastic deflection as shown in Fig. 8 ranked in the order of HVOF Al_2O_3 < plasma-sprayed Al_2O_3 < B_4C–C composite < Al_2O_3–C composite = Al_2O_3–B_4C composite = B_4C < $MgAl_2O_4$ < Al–C. In summary, the impact tests of thermally-sprayed coatings on aluminum panels exhibited composite mechanical response under impact loading. Local deflection was affected by the adherence and compressive strength of the ceramic coating. All coating materials exhibited significant inelastic deflection prior to visible spallation damage. Coating failure was strongly affected by deformation of the aluminum panel. Conversely, deformation of the aluminum panel was strongly influenced by failure of the coating. The type and periodicity of back-face support will affect the impact performance of ceramic-coated aluminum panels.

Conclusion

Plasma spray deposition of B_4C using APS without cryogenic cooling of the substrate was successful but required argon jet shrouds and a standoff distance of 50.8 mm (2.0 in.). This approach may help optimize particle time in the molten state, produce more uniform cooling rates for various size particles, reduce carbon redistribution, and reduce residual stress variations from splat to splat. Good relative tensile

strengths were achieved using graded bond coats. An excellent match to the PDF XRD file was obtained showing B_4C coatings without significant boric oxide or boric acid formation. RBS results indicated that stoichiometric B_4C was deposited using the argon-jet-shrouded APS process. The CO_2 pellet cleaning and erosion tolerance studies showed that surface cleaning was easily achieved without significant damage and that the B_4C coatings exhibited good erosion tolerance performance. The thermal shock loading with a drop in temperature from 150°C to 0°C resulted in some change in thermal diffusivity for the plasma-sprayed coatings of B_4C and B_4C composites, which suggested either a small amount of delamination or microcracking. The B_4C and B_4C composite coatings exhibited good impact resistance, showing incipient spallation at ~2.8 kg•m/s and momentum greater than 4 kg•m/s before the cumulative inelastic deflection exceeded 1.0 mm. Composite mechanical response under impact loading was exhibited for the impact tests of the thermally-sprayed coatings on aluminum panels. All coating materials exhibited significant inelastic deflection prior to visible spallation damage.

Acknowledgment

A number of individuals performed key characterizations, evaluations, or tests as noted below. G. Garrison, R. Dinwiddie, G. Romanoski, J. Haines, and M. McFee of Oak Ridge National Laboratory coordinated the routing of the samples for various studies and maintained a log of the data, performed the prethermal and postthermal diffusivity measurements for the thermal shock evaluations and evaluated the data, completed the low-velocity impact tests and analyzed the data, conducted the CO_2 pellet cleaning and erosion resistance tests, and conducted several DECTAK profile measurements, respectively. J. Mabon, L. Thompson, D. Carpenter, and L. Ratcliff of the Oak Ridge Y-12 Plant performed the optical microscopy and SEM work, completed the relative tensile strength tests, conducted the X-ray diffraction analysis, and assisted with sample preparation for optical microscopy, respectively. M. Tobin, LLNL, provided the RBS data and coordinated X-ray tolerance testing.

References

1 Tobin, M. T., 12th Topical Meeting on the Technology of Fusion Energy, 1996.

2 van der Laan, J. G., G. Schnedecker, E. V. van Osch, R. Duwe, J. Linke, J. Nucl. Materials, 211, 135–140 (1994).

3 Massalski, T. B., "Binary Alloy Phase Diagrams," American Society for Metals (1986).

4 Elliott, R. P., "Constitution of Binary Alloys," McGraw-Hill (1965).

5 Shaffer, P. T. B., "Engineering Properties of Carbides," ASM Engineered Materials Handbook, 4, 804 (1991), S. J. Schneider, Jr., Vol. Chairman.

6 Mallener, W., and D. Stover, Proc. of the 1993 National Thermal Spray Conference, Anaheim, CA, June 7–11, 1993, pp. 291–295.

7 Mallener, W., H. J. Grob, D. Stover, Proc. of the 7th National Thermal Spray Conference, June 20–24, 1994, pp. 627–632.

DISCLAIMER